Biochimica et Biophysica Acta 1788 (2009) 1009–1023

Contents lists available at ScienceDirect

Biochimica et Biophysica Acta

journal homepage: www.elsevier.com/locate/bbamem

Forces and stresses acting on fusion pore membrane during secretion

M. Tajparast [a], M.I. Glavinović [b,*]

[a] Department of Civil Engineering, McGill University, Montreal, PQ, Canada
[b] Department of Physiology, McGill University, 3655 Sir William Osler Promenade, Montreal, P.Q. Canada H3G 1Y6

ARTICLE INFO

Article history:
Received 23 August 2008
Received in revised form 7 January 2009
Accepted 30 January 2009
Available online 11 February 2009

Keywords:
Fusion pore
Exocytosis
Membrane
Navier–Stokes
Lipid
Pore dynamics
Tension

ABSTRACT

To assess the forces and stresses present in fusion pore during secretion the stationary convective flux of lipid through a fusion pore connecting two planar membranes under different tensions was investigated through computer simulations. The physics of the problem is described by Navier–Stokes equations, and the convective flux of lipid was evaluated using finite element method. Each of the membrane monolayer is considered separately as an isotropic, homogeneous and incompressible viscous medium with the same viscosity. The difference in membrane tensions, which is simulated as the pressure difference at two ends of each monolayer, is the driving force of the lipid flow. The two monolayers interact by sliding past each other with inter-monolayer frictional viscosity. Fluid velocity, pressure, shear and normal stresses, viscous and frictional dissipations and forces were calculated to evaluate where the fusion pore will deform, extend (or compress) and dilate. The pressure changes little in the planar sections, whereas in the toroidal section the change is rapid. The magnitude of lipid velocity peaks at the pore neck. The radial lipid velocity is zero at the neck, has two peaks one on each side of the pore neck, and diminishes without going to zero in planar parts of two monolayers. The peaks are of opposite signs due to the change of direction of lipid flow. The axial velocity is confined to the toroidal section, peaks at the neck and is clearly greater in the outer monolayer. As a result of the spatially highly uneven lipid flow the membrane is under a significant stress, shear and normal. The shear stress, which indicates where the membrane will deform without changing the volume, has two peaks placed symmetrically about the neck. The normal stress shows where the membrane may extend or compress. Both, the radial and axial normal stresses are negative (extensive) in the upper toroidal section and positive (compressive) in the lower toroidal section. The pressure difference determines lipid velocity and velocity dependent variables (shear as well as normal axial and radial stresses), but also contributes directly to the force on the membranes and critically influences where and to what extent the membrane will deform, extend or dilate. The viscosity coefficient (due to friction of one element of lipid against neighboring ones), and frictional coefficient (due to friction between two monolayers sliding past each other) further modulate some variables. Lipid velocity rises as pressure difference increases, diminishes as the viscosity coefficient rises but is unaffected by the frictional coefficient. The shear and normal stresses rise as pressure difference increases, but the change of the viscosity coefficients has no effect. Both the viscous dissipation (which has two peaks placed symmetrically about the neck) and much smaller frictional dissipation (which peaks at the pore neck) rise with pressure and diminish if the viscosity coefficient rises, but only the frictional dissipation increases if the frictional coefficient increases. Finally, the radial force causing pore dilatation, and which is significant only in the planar section of the vesicular membrane, is governed almost entirely by the pressure, whereas the viscosity and frictional coefficients have only a marginal effect. Many variables are altered during pore dilatation. The lipid velocity and dissipations (viscous and frictional) rise approximately linearly with pore radius, whereas the lipid mass flow increases supra-linearly owing to the combined effects of the changes in pore radius and greater lipid velocity. Interestingly the radial force on the vesicular membrane increases only marginally.

1. Introduction

In the exocytosis of hormones, transmitters or peptides the fusion pore, which forms by mixing two biological membranes previously separated, links the vesicular interior with the extracellular fluid providing a conduit for the secretion of the vesicular content [1]. Dynamics of opening and closing of the fusion pore can be an important factor in regulating the amount and the time course of release of vesicular content and thus in determining the quantal size [2,3]. However, there are many unanswered questions about what controls fusion pore dynamics. Although the electrical recordings of the fusion pores and ion channels are similar [4], it is still controversial whether their composition is also similar [5–9]. Whereas the ion

* Corresponding author. Tel.: +1 514 398 6002; fax: +1 514 398 7452.
E-mail address: mladen.glavinovic@mcgill.ca (M.I. Glavinović).

0005-2736/$ – see front matter © 2009 Elsevier B.V. All rights reserved.
doi:10.1016/j.bbamem.2009.01.019

channels are formed of well-characterized proteins, recent studies suggest that the fusion pore may be a lipoprotein structure incorporating soluble *N*-ethylmaleimide-sensitive factor attachment protein receptors (SNAREs) [10,11]. The fusion pore is thus envisioned as a lipoprotein, with lipid moving between membranes soon following the pore formation and increasing as the pore grows.

The exocytotic granule membranes are under significantly greater tension than plasma membranes [12,13], and this difference in tension drives the lipid movement [14] and may induce forces critically influencing the pore dynamics. The difference in tension is opposed by the dissipative forces due to the shear viscosity and by the inter-monolayer friction (which arises from viscous friction between monolayers as they slip past each other and is described with a friction coefficient). The inter-monolayer friction and shear, which determine the membrane flow, appear themselves to be controlled by the proportion of lipids and sterols in the membrane of living cells [15]. Whereas the friction between a monolayer and the bathing aqueous solution is negligibly small, the inter-monolayer friction can be substantial. The inter-monolayer friction coefficients can be calculated from measurements or simulations of membranes undergoing parallel shear, which forces the two membrane leaflets to slide past one another. The friction coefficient is calculated as the ratio between the friction force per unit area and the slip velocity. Alternatively, the friction coefficient can be estimated from analyzing the relaxation rates of thermal membrane undulations using the Seifert–Langer theory [16]. Both approaches give similar results.

Energy dissipation due to shear deformations results from lipid–lipid and lipid–protein interactions within each monolayer, and is characterized by a shear viscosity coefficient defined as the proportionality constant between the applied shear rate and the corresponding shear force acting on the bilayer per unit length [17]. The experimental estimates of the surface shear viscosities of membranes are based on a theory relating the surface shear viscosity to the translational diffusion coefficient of a tracer particle confined to a membrane (analogous of the Stokes–Einstein relation; [18]). These shear viscosity measurements use labeled membrane-bound proteins as the diffusing tracer particle [19,20], latex spheres [21–23] and phase-separated lipid domains [24].

Previous theoretical studies provided important insights into the mechanism of generation of lipid flow and viscous and frictional dissipation induced by the tension difference between the vesicular and plasma membranes [5–8,14]. However, further progress, which is needed to evaluate how the dynamics of the fusion pore–planar membrane complex is controlled by the tension difference and how the pore may dilate, deform or extend, requires a numerical evaluation. The stationary convective flux of lipids resulting from the tension difference between the vesicular and plasma membranes was simulated using finite element method, and the lipid velocity, pressure, shear stress and normal stresses in the membrane and finally the forces acting on the fusion pore–planar membrane complex were calculated. Finite element method is needed whenever the geometry of the system and boundary conditions are not very simple (i.e. when the methods based on highly idealized geometries and mechanical properties are not suitable). It has been used successfully for analysis of molecular motors [25], for evaluation of mechano-sensitive channel gating [26], and for transport of water, ions and glutamate in charged nanosize slit pores [27] or cylindrical pores [28].

2. Methods

2.1. Geometry

The computational domain consisting of the plasma and vesicular membranes and the fusion pore has a cylindrical geometry (Fig. 1; A — Side view of the schematic diagram of the system in r–z plane; B — Top view of the model in r–θ plane). R — the radius where the toroidal pore and planar membranes meet ranges from 11.0 to 18.0 nm; r_p — the radius of the narrowest portion of the fusion pore lumen ranges from 1.0 nm to 8.0 nm; h — the thickness of the monolayer is 3.0 nm; L — the separation between the membrane mid-lines of the parallel sections is 7.0 nm, and is determined by the choice of the thickness of the monolayers and by their separation, and determines the curvature radius of the stalk in the r/z plane. The monolayer thickness is unlikely to change during secretion. Although the separation between monolayers may change during secretion [29], in this study we assumed that it is constant. The length of each planar membrane section was 88 nm. The bold solid lines illustrate membrane-solution interfaces. The thin solid lines depict the interfaces between monolayers.

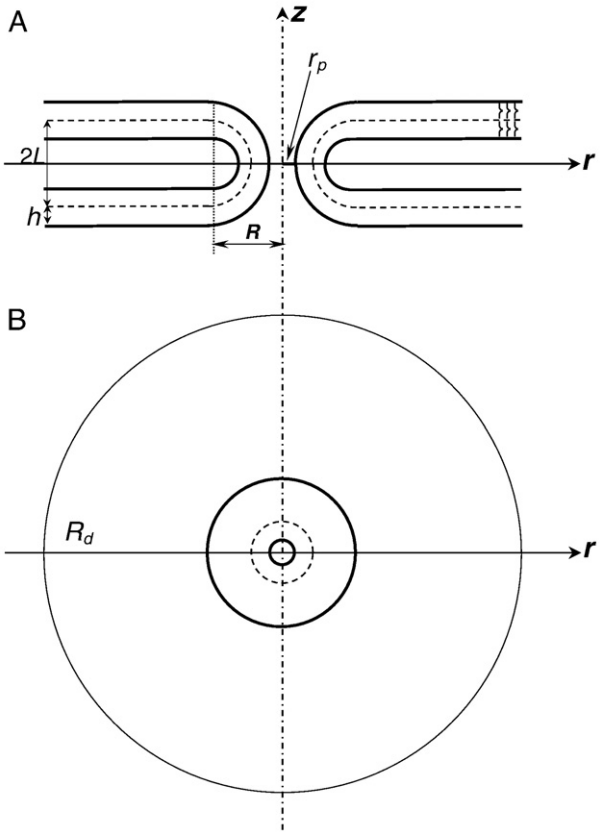

Fig. 1. Schematic diagram of a fusion pore connecting two planar membranes at different tensions. Cross-sectional view of the pore in z, r coordinates. The membrane–solution interfaces are indicated as bold solid lines. The dotted line depicts the interface between monolayers. The radius R indicates the distance from the pore center to where the pore toroidal section and planar membranes meet, whereas r_p is the radius of the narrowest portion of the fusion pore lumen. R_d denotes the far ends of the planar membrane, h indicates the thickness of a monolayer, whereas L is the half-distance between the vesicular and planar surfaces where two monolayers slide past each other. (A) Side view. (B) Top view of the model in r–θ plane.

2.2. Governing equations, parameters, and boundary conditions

We consider each monolayer as a homogeneous, isotropic incompressible fluid, thus without making a distinction between the hydrophobic tail regions and the polar heads. The unsteady Navier–Stokes equation, in the absence of external forces, describes the fluid behaviour in the planar and toroidal parts of the fusion pore as follows [30]:

$$\rho\left(\frac{\partial \mathbf{u}}{\partial t} + \mathbf{u}.\nabla\mathbf{u}\right) = -\nabla p + \mu\nabla^2\mathbf{u} \quad (1)$$

$$\nabla.\mathbf{u} = 0 \quad (2)$$

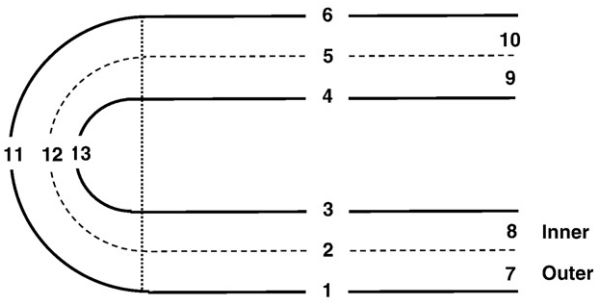

Fig. 2. Hemisection of the computational domain with boundaries. No-penetration boundary condition is applied on the membrane–solution interfaces enclosing the parallel planar membranes (boundaries 1–6). At the far ends of the system (boundaries 7–10) constant pressure is applied, but their values are not fixed and are determined by the simulations. Instead a chosen pressure difference between two ends of each monolayer (7 and 10 — the outer monolayer, and between ends 8 and 9 — the inner monolayer) is applied. The pressure difference is the same for both monolayers, but changes from one simulation to another. The toroidal section of the fusion pore is enclosed by two boundaries (boundaries 11 and 13) with no-penetration boundary condition. On boundaries 2, 5 and 12, there is a friction between two monolayers (see text).

Eq. (1) describes the conservation of momentum, while Eq. (2) accounts for the conservation of mass. ρ, μ, and p are the fluid density, viscosity and pressure, respectively, and the vector **u** denotes the fluid velocity. These equations are applied to both the outer and inner monolayer. The fluid density $\rho = 915$ kg/m^3, and viscosity $\mu = 5*10^{-2}$ Pa s (or as specified), whereas the friction coefficient at the interface of two monolayers is $\mu_f = 5.0*10^8$ Pas/m (or as specified).

The computational domain contains thirteen boundaries (Fig. 2). On boundaries 1–6 enclosing the parallel planar membranes, we apply no-penetration boundary condition. Boundaries 7–10 are the far ends of the system with constant pressure, but their values are such to ensure a chosen pressure difference between two ends of each monolayer [7 and 10 — the outer monolayer, and between ends 8 and 9 — the inner monolayer), which may change from one simulation to another (see Results). Boundaries 11–13 enclose the toroidal portion of the fusion pore model with no-penetration boundary conditions. On boundaries 2, 5 and 12, there is a friction between two monolayers.

3. Results

3.1. Spatial distribution of lipid velocity

The evaluation of lipid velocity in each of the monolayer is essential for the understanding of the viscotic stress, viscous and frictional dissipation and forces acting on the monolayers. The magnitude of lipid velocity peaks in the pore neck, but the peak value in the outer monolayer is significantly greater than in the inner monolayer (Fig. 3A–C). The axial velocity is: a) always positive, b) peaks at the neck for both monolayers, c) clearly greater for the outer monolayer, and d) zero in the planar section for both monolayers (Fig. 3D). In contrast the radial lipid velocity has two peaks, one on each side of the pore neck, which are of opposite signs due to the change of direction of the radial velocity. Moreover, the radial velocities in two monolayers, though not identical are similar in value. Both diminish without going to zero in planar parts of two monolayers, as do the velocity magnitudes, which are almost identical to the radial velocities (the axial velocities are zero). The pressure difference at the ends of individual monolayers strongly affects the lipid velocity (Fig. 3E), which increases linearly with the rise of the pressure difference (Fig. 3H). The lipid velocity is however insensitive to changes of the friction coefficient even when they are very large (Fig. 3G, H). However, the velocity depends on the viscosity coefficient, and the relationship is inverse (Fig. 3F and H).

3.2. Spatial distribution of shear and normal stresses

Spatially uneven lipid velocity profiles indicate that both the shear and normal stress should also be spatially uneven. Fig. 4A depicts how the shear stress changes along the arc going through the middle of the inner and outer monolayers. Indeed, the shear stress changes largely in the toroidal region, and is greater in the outer monolayer. The peaks are placed symmetrically from the central point at the pore neck, which is positioned parallel to the axis of symmetry, and where the shear stress is zero (see Discussion). Further along the arc the shear stress rapidly diminishes to the zero level in the planar membrane sections. The pressure difference at the ends of individual monolayers affects the amplitude of the shear stress, although its spatial distribution remains the same (Fig. 4B and E). In contrast neither the amplitude nor the spatial distribution of the shear stress is altered by the changes of viscosity or friction coefficients (Fig. 4C–E).

The axial normal stress is zero in the planar membrane sections, changes very rapidly in the toroidal section, and is greater in the outer than in the inner monolayer (Fig. 5A). Whereas the axial normal stress is positive (compressive) in the lower part of the toroidal section it is negative (extensive) in the upper part. The peak axial normal stress rises linearly with a rise of the pressure difference at the ends of individual monolayers, although its spatial distribution remains the same (Fig. 5B and E). Neither the amplitude nor the spatial distribution of the axial normal stress is altered by the changes of viscosity or friction coefficients (Fig. 5C–E).

The spatial distribution of the radial normal stress is similar to that of the axial normal stress, but is less confined to the toroidal section (Fig. 6A). Like the axial normal stress, the radial normal stress is positive (compressive) in the lower part of the toroidal section but negative (extensive) in the upper part of the toroidal section. However, the differences between the radial normal stress in the inner and outer monolayer are minimal. The peak radial normal stress also rises linearly with a rise of the pressure difference at the ends of individual monolayers, although its spatial distribution remains the same (Fig. 6B and E). In addition, neither the amplitude nor the spatial distribution of the axial normal stress is altered by the changes of viscosity or friction coefficients (Fig. 6C–E).

3.3. Spatial distribution of pressure

The pressure difference at two ends of each monolayer is the driving force of lipid flow, but what is its spatial profile in the fusion pore–membrane complex? Fig. 7A, B gives the tri-dimensional pressure profiles, whereas Fig. 7C depicts the pressure distribution along the arc running through the middle of the inner and outer monolayer. The pressure changes little in the planar sections, whereas in the toroidal section it changes rapidly, from near a zero level in the lower planar section ('plasma membrane') to the negative, but a high value level in the upper planar section ('vesicular membrane'). The pressure in the vesicular membrane changes when the pressure difference at two ends of each monolayer changes, but the shape of the spatial distribution remains largely the same. The pressure however, is generally lower, though not greatly in the inner monolayer. Finally the pressure distributions remain the same if the viscosity or friction coefficients are altered (Fig. 7D, E), but if the radius of the fusion pore changes from 2 to 4 nm the pressure distribution is altered (Fig. 7F).

3.4. Distribution of viscous and frictional dissipation

The viscous and frictional dissipations oppose the pressure difference, and to evaluate their importance it is essential to determine not only the shape of their distributions, but the amplitude as well. Fig. 8G shows how the distributions of the viscous dissipation per unit volume, and the viscous dissipation change along the arc

running through the middle of the inner or outer monolayer. Both distributions display two peaks, each on one of the sides of the valley whose minimum is located at the neck of the pore. Owing to the geometrical factors the viscous distribution extends, though only modestly into the planar sections (see Discussion). Moreover, both viscous dissipation and viscous dissipation per unit volume are greater in the outer monolayer. They rise supra-linearly (without changing their shape) as the pressure difference at the ends of individual

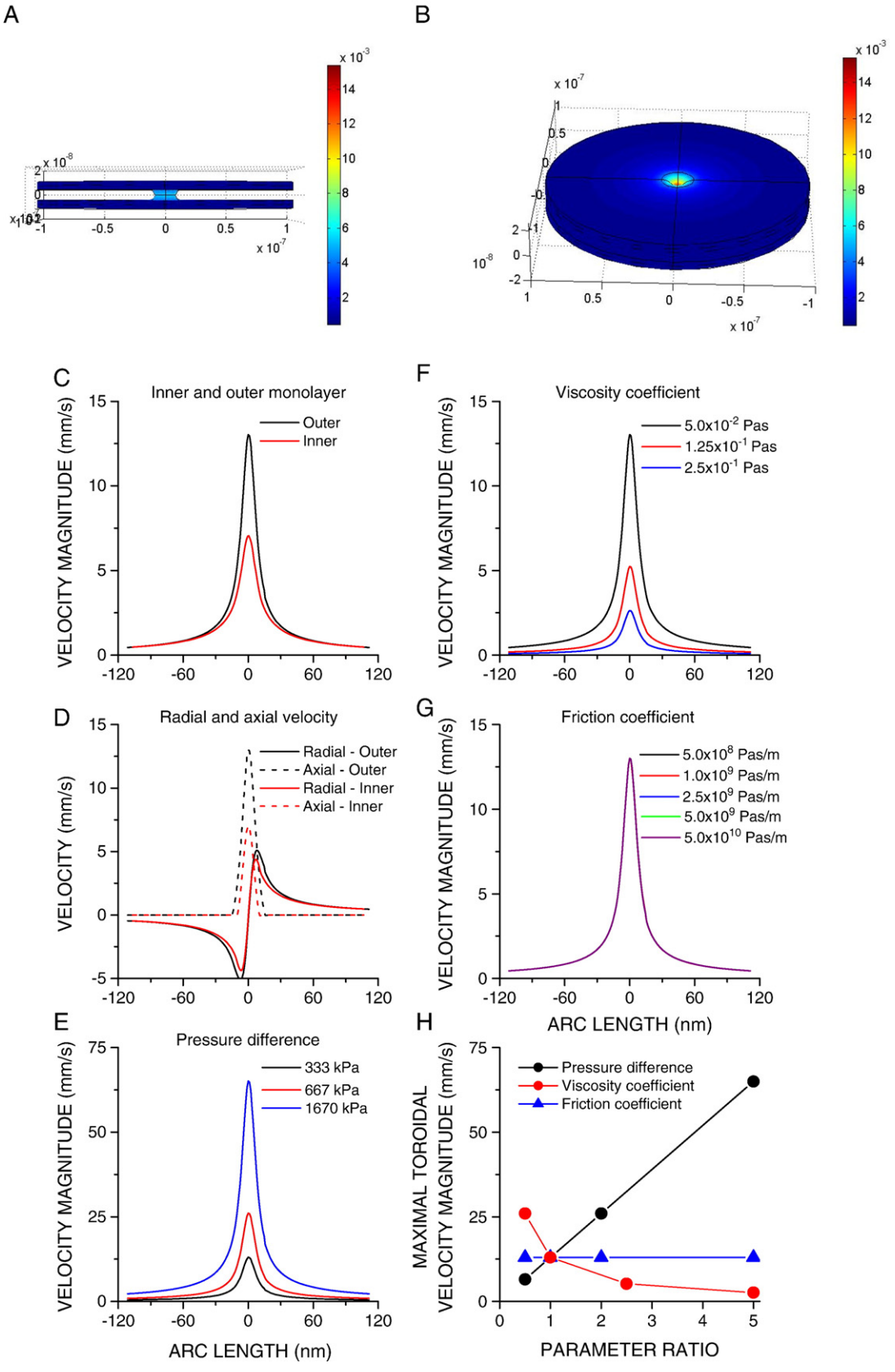

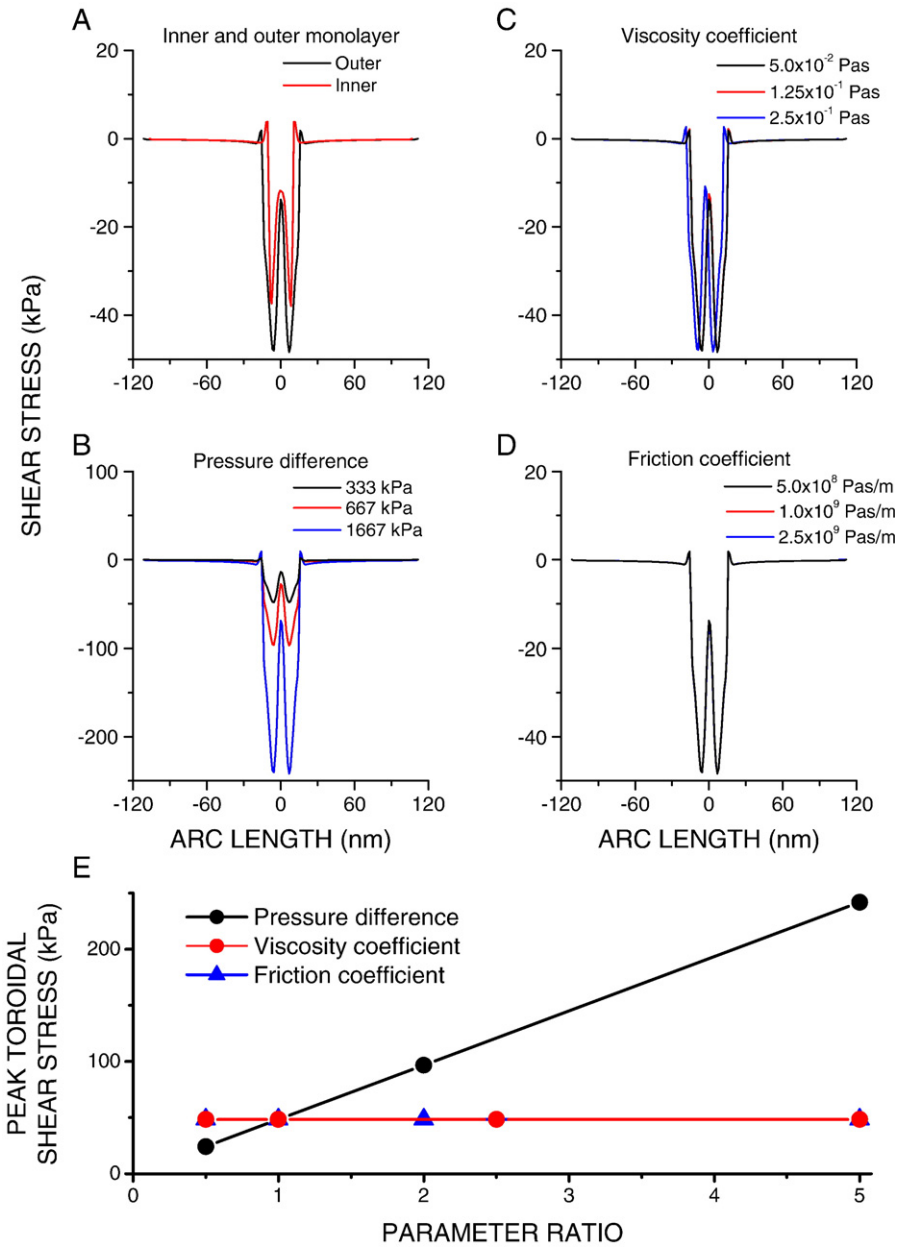

Fig. 4. (A) Shear stress along the arc of the inner and outer monolayers is near zero at the neck, displays two peaks on each side of the neck, but is zero in the planar section for both monolayers. The shear stress is greater in outer monolayer. (B–D) The pressure difference at the ends of each monolayer affects the shear stress significantly, whereas the viscosity and friction coefficients alter it only marginally. (E) The relationship between the peak toroidal shear stress and the ratio of different parameters. The ratio of one indicates the simulation with the pressure difference at the ends of monolayers of 333 kPa, viscosity coefficient of $5*10^{-2}$ Pa s, and friction coefficient of $5.0*10^{8}$ Pas/m. All plots (except A) depict the shear stress from the outer monolayer.

monolayers increases (Fig. 8A, B and H). In contrast they diminish if the viscosity coefficient rises (Fig. 8C, D and H). If the friction coefficient changes they are not altered significantly (Fig. 8E–F and H).

Fig. 9A, B shows the distribution of the frictional dissipation per unit area and of the corresponding frictional dissipation and how they depend on the pressure difference at the ends of individual monolayers. Both distributions have one prominent and narrow peak at the neck of the fusion pore due to the fact that the difference of the lipid velocity at two sides from the surface where two monolayers slide past each other is typically greatest at the neck, becoming zero short distance from the neck (Fig. 9G). Both distributions rise without changing their shape as the pressure difference at the ends of

Fig. 3. (A–B) Three-dimensional depiction of the magnitude of the lipid velocity (all dimensions are given in meters and velocity in meter/second; A — front view; B top view). (C) Magnitude of the lipid velocity along the arc length in the middle of the inner and the outer monolayers is maximal at the pore neck, and the peak value in the outer monolayer is significantly greater than in the inner monolayer. (D) In both monolayers the radial lipid velocity has two peaks but of the opposite signs, one on each side of the pore neck. Note that the radial velocities in two monolayers are similar in value and diminish without going to zero in planar sections of two monolayers. In contrast in the toroidal section the axial velocity is always positive, peaks at the neck for both monolayers, and is clearly greater for the outer monolayer, whereas in the planar section it is zero for both monolayers. (E, F) The velocity magnitude increases as the pressure difference at the ends of each monolayer rises, but diminishes as the viscosity coefficient rises. (G) The velocity magnitude is unaffected by the change of the friction coefficient. (H) The relationship between the maximal toroidal velocity magnitude and the ratio of different parameters. The ratio of one indicates the simulation with the pressure difference at the ends of monolayers of 333 kPa, viscosity coefficient of $5*10^{-2}$ Pa s, and friction coefficient of $5.0*10^{8}$ Pas/m. All plots (except C) depict velocities from the outer monolayer.

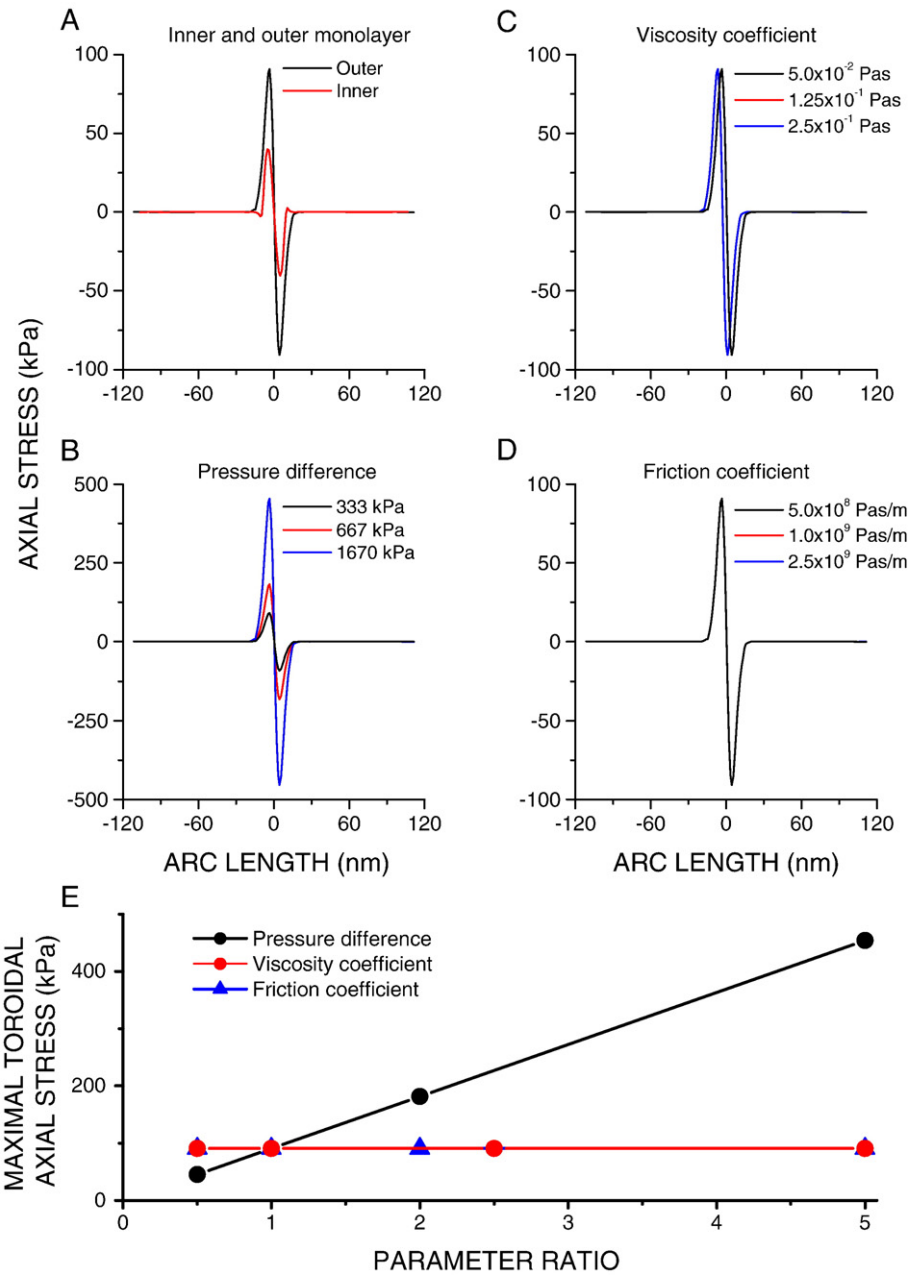

Fig. 5. (A) Axial normal stress peaks in the toroidal section on both sides of the pore neck, but is positive (compressive) in the lower part of the toroidal section and negative (extensive) in the upper part, whereas in the planar section it is zero for both monolayers. The axial normal stresses of two monolayers differ, being greater (more compressive in the lower part, and more extensive in the upper part) in the outer monolayer. (B–D) The pressure difference at the ends of each monolayer affects the axial stress significantly, whereas the viscosity and friction coefficients alter it only marginally. (E) The relationship between the maximal toroidal axial stress and the ratio of different parameters. The ratio of one indicates the simulation with the pressure difference at the ends of monolayers of 333 kPa, viscosity coefficient of $5*10^{-2}$ Pa s, and friction coefficient of $5.0*10^{8}$ Pas/m. All plots (except A) depict the axial normal stress from the outer monolayer.

individual monolayers increases (Fig. 9A, B), and the rise of the frictional dissipation is supra-linear (Fig. 9H). They diminish if the viscosity coefficient rises (Fig. 9C, D and H). If the friction coefficient rises, the frictional dissipation rises linearly (Fig. 9E, F and H). Nevertheless, note that a tenfold rise of the friction coefficient is associated with a smaller (6.9 times) rise of the frictional dissipation. Finally, the frictional dissipation is much smaller than viscous dissipation.

3.5. Radial and axial force distributions

The force acting on the fusion pore–membrane complex is a result of the 'external' force (pressure difference) and the 'internal' force opposing it due to the viscous dissipation (see Appendix). Fig. 10A, B depicts the distributions of the radial force per unit area and radial force at the external boundary of the outer monolayer for three different pressure differences at the ends of individual monolayers. Note that given the monolayer thickness of 3 nm, the pressure difference of 333 kPa corresponds to the tension difference of 1 dyne/cm (see Appendix). Even in the simulations with the greatest pressure difference (1667 kPa) this corresponds to the tension difference of 5 dyne/cm, thus clearly below the membrane rupture threshold of ~15 dyne/cm. The viscotic (magenta) and pressure (purple) contributions to the radial force per unit area are also shown for the simulation with the greatest pressure difference at the monolayer ends (1667 kPa). The pressure contribution clearly

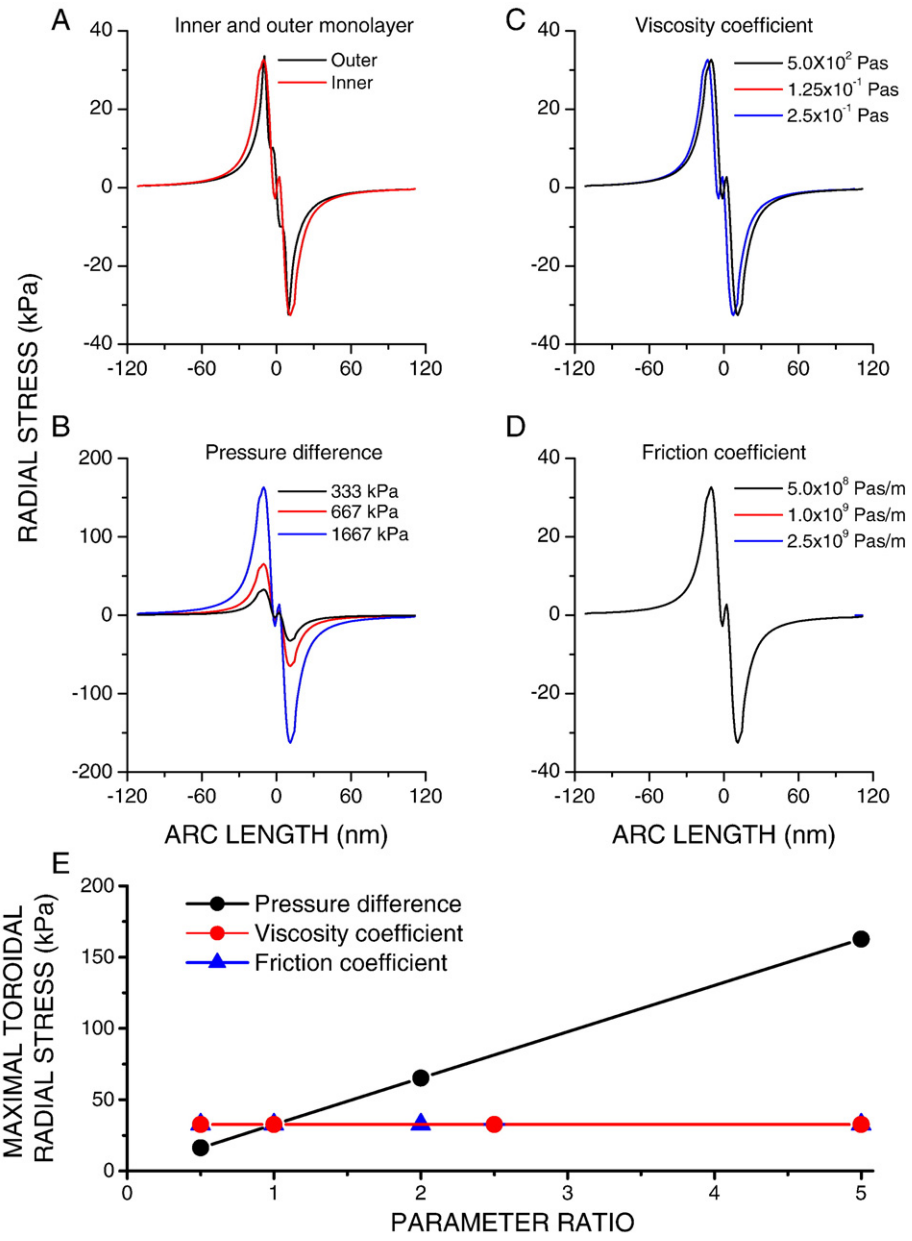

Fig. 6. (A) Radial normal stress peaks in the toroidal section on both sides of the pore neck, but is also positive (compressive) in its lower part and negative (extensive) in its upper part, whereas in the planar section it gradually declines to zero for both monolayers. The radial normal stresses of two monolayers are similar throughout the fusion pore–planar membranes complex. (B–D) The pressure difference at the ends of each monolayer affects the radial stress significantly, whereas the changes of the viscosity and friction coefficients alter it only marginally. (E) The relationship between the maximal toroidal radial stress and the ratio of different parameters. The ratio of one indicates the simulation with the pressure difference at the ends of monolayers of 333 kPa, viscosity coefficient of $5*10^{-2}$ Pa s, and friction coefficient of $5.0*10^{8}$ Pas/m. All plots (except A) depict the radial normal stress from the outer monolayer.

predominates, whereas the viscotic contribution is quite small. Note that the radial force per unit area is in general close to zero in the lower planar section, whereas in the upper planar section it is nearly constant and high (how high it is depends on the pressure difference at the ends of monolayers). Consequently the greater the external pressure the greater the slope of the radial force vs. arc length relationship (Fig. 10B). In contrast the viscosity and friction coefficients have no effect on the radial force (Fig. 10C–F). We also calculated the total radial force at the external boundary of the outer monolayer (the pressure difference at the ends of individual monolayers was 333 kPa, the viscosity coefficient was $5*10^{-2}$ Pa s and the friction coefficient was $5.0*10^{8}$ Pa s) within a chosen distance from the end at the plasma membrane (Fig. 10G). If the fusion pore is associated with a large vesicle, and if the tension difference between the vesicular and plasma membranes is maintained the radial force will be significant, but if the vesicle is small the radial force will be much smaller.

Fig. 11A–C depicts the spatial distribution of the axial force at the external boundary of the outer monolayer for different pressure differences at the ends of individual monolayers and for different viscosity and friction coefficients. The axial force is much smaller than radial force, but like radial force it depends on the pressure difference, but not on the value of either viscosity or friction coefficients.

3.6. Fusion pore dilatation

The fusion pore dilatation will change the balance of forces in the fusion pore–membrane complex, and thus the variables determining the lipid flow, but how much will each variable change? Fig. 12 shows the changes of lipid velocity, stress, forces and lipid mass flow

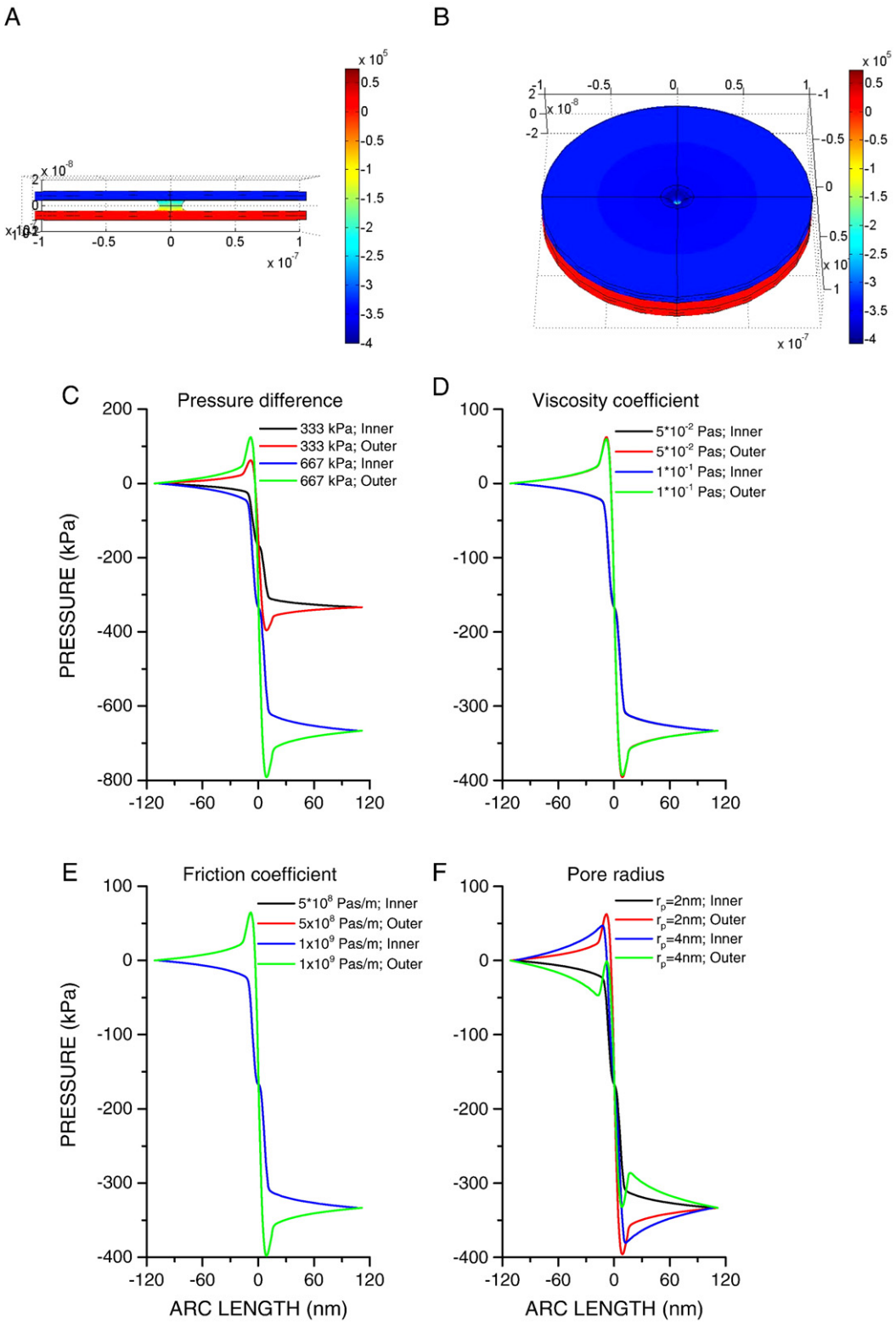

Fig. 7. (A, B) Three-dimensional depiction of pressure (all dimensions are given in meters and pressure in Pascal; A — front view; B top view). (C) Pressure along the arc running through the middle of the inner and outer monolayers changes moderately in the planar sections, but rapidly in the toroidal section, whereas in the outer and the inner monolayers it is different though not greatly. The pressure difference at the ends of each monolayer determines the pressure in the vesicular membrane, whereas in the plasma membrane the pressure remains close to zero. (D, E) Neither the viscosity coefficient nor friction coefficient affects the pressure distribution profiles. (F) The pressure profile depends on the pore radius but only moderately.

associated with pore dilatation. As the pore radius increases the lipid velocity rises (the maximal toroidal velocity, mean total velocity and mean velocity estimated at the end of each monolayer; Fig. 12A). The peak value of the shear stress in the toroid also rises, very modestly for the outer monolayer, but significantly for the inner monolayer surpassing the value in the outer monolayer when pore radius increases beyond 4 nm (Fig. 12B). Both the total viscous and total frictional dissipations increase approximately linearly with pore

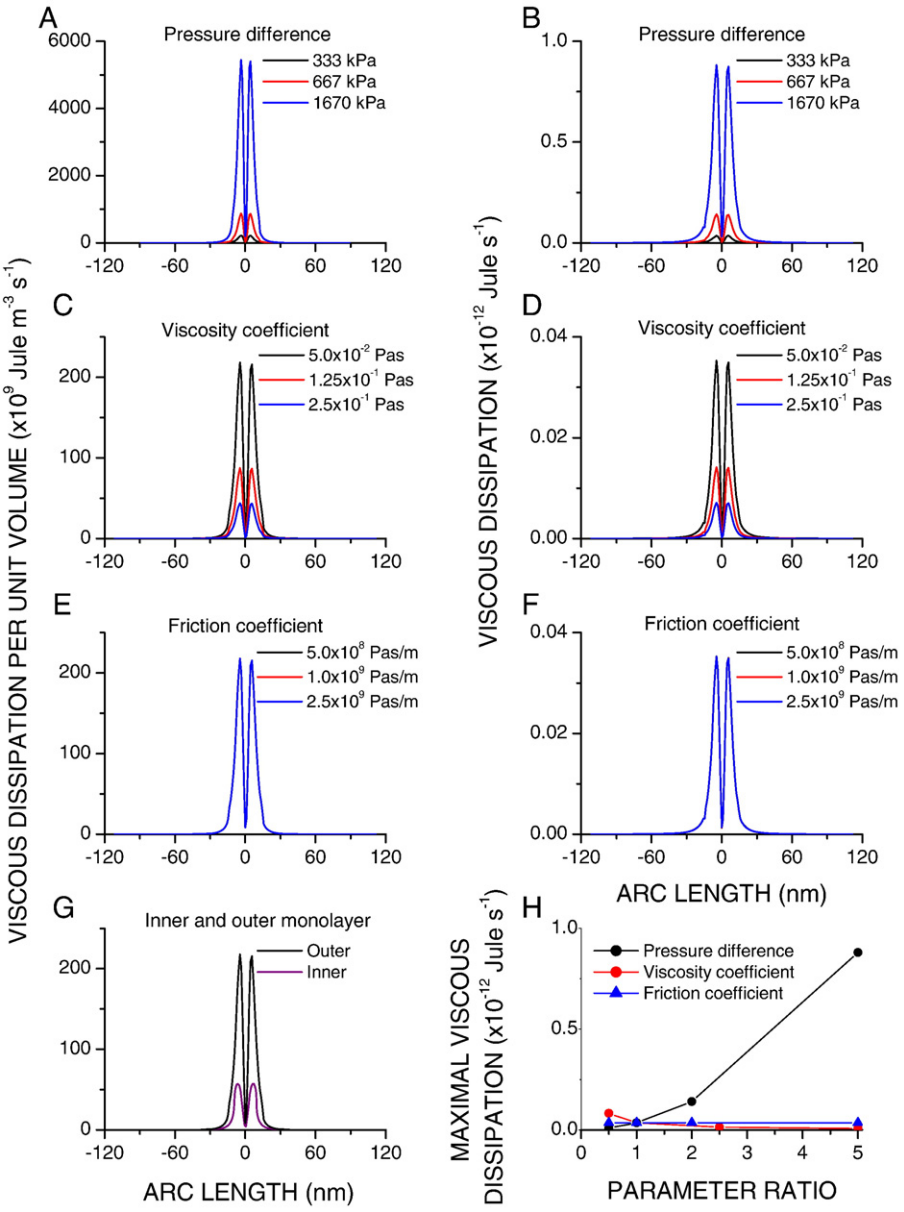

Fig. 8. Viscous dissipation per unit volume distribution (A), and viscous dissipation distribution (B) along the arc running through the middle of the outer monolayer. Both distributions have two peaks, each on one of the sides of the valley whose minimum is at the pore neck. Owing to the geometrical factors the viscous distribution is wider and extends into the planar sections (see text). The pressure at the ends of the monolayers powerfully affects the viscous dissipation. (C, D) The viscous dissipation and the viscous dissipation per unit volume diminish as the viscosity coefficient rises. (E, F) Friction coefficient does not affect the viscous dissipation (or viscous dissipation per unit volume). (G) Viscous dissipation is significantly greater in the outer than in inner monolayer. (H) The relationship between the maximal viscous dissipation and the ratio of different parameters. The ratio of one indicates the simulation with the pressure difference at the ends of monolayers of 333 kPa, viscosity coefficient of $5*10^{-2}$ Pa s, and friction coefficient of $5.0*10^{8}$ Pas/m. All plots (except G) depict the viscous dissipation from the outer monolayer.

radius. Note however, that the total viscous dissipation of both monolayers combined is independent of even a large increase of friction coefficient, but such an increase renders the total frictional dissipation much greater (Fig. 12C, D). The total radial force rises linearly, but modestly as the pore radius increases (Fig. 12E). Finally the dependence of the mass flow on the pore radius is quite pronounced and approximately linear, and its values are similar in both monolayers (Fig. 12F).

4. Discussion

4.1. Lipid velocity and frictional dissipation

The starting point for better understanding of the effects of the lipid flow on stress, energy dissipation and force on the membrane is the estimation of the spatial distribution of lipid velocity — its magnitude and its radial and axial components, because the spatial distribution of these variables is determined by lipid velocity and its profile (see Methods). As suggested previously [14] the magnitude of lipid velocity peaks at the fusion pore neck. Because the lipid traverses a longer pathway in the outer than in the inner monolayer the difference in magnitude of velocity between two monolayers is also the greatest at the neck. Velocity magnitude diminishes as the fluid viscosity rises, but does not change even when its friction coefficient increases 100 times. This is not surprising given that the fluid velocities of the inner and outer monolayers near their interface differ only at the neck of the toroid, even when the friction coefficient is low ($5.0*10^{8}$ Pas/m). The difference of the velocity magnitude is largely due to the differences of the axial velocity, which is confined exclusively to the toroidal section, and is

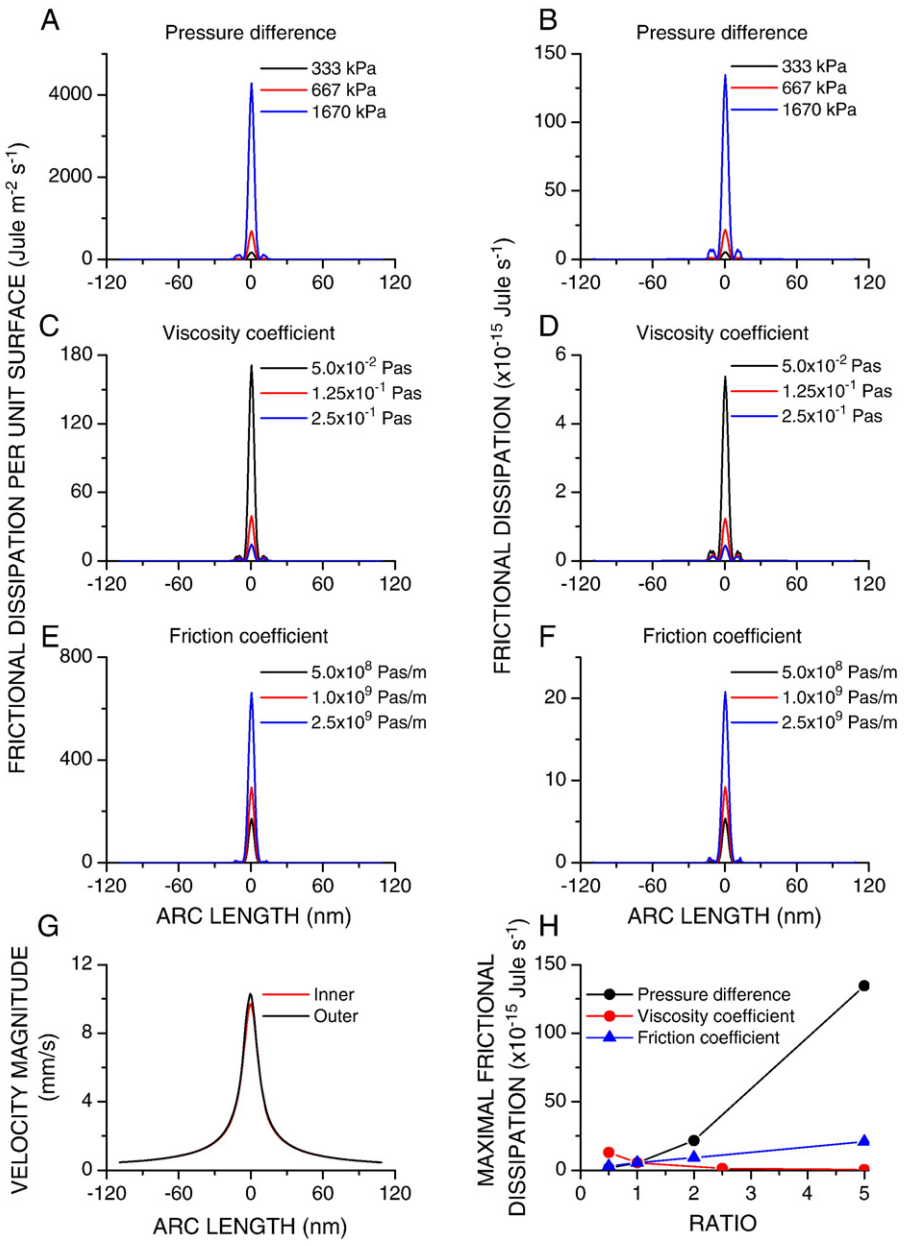

Fig. 9. (A) Frictional dissipation per unit area distribution is confined to the toroidal section, and has a sharp peak at the pore neck. (B) Frictional dissipation distribution is wider, but only moderately (see text). The pressure difference at two ends of each monolayer influences greatly the frictional dissipation, which rises as the pressure difference increases. (C, D) The viscosity coefficient also has a strong effect on the frictional dissipation, but the relationship is inverse. (E, F) Increasing the friction coefficient renders the frictional dissipation moderately greater. (G) Comparison of the velocity magnitude profiles (estimated 0.1 nm away from the boundary between two monolayers on each side) illustrates why the frictional dissipation has a very sharp peak at the pore neck. (H) The relationship between the maximal frictional dissipation and the ratio of different parameters. The ratio of one indicates the simulation with the pressure difference at the ends of monolayers of 333 kPa, viscosity coefficient of $5*10^{-2}$ Pa s, and friction coefficient of $5.0*10^{8}$ Pas/m. All plots depict the frictional dissipation at the interface of two monolayers.

zero in planar sections. The radial velocity changes the direction in the toroidal section, and its value is also the greatest (though opposite in direction) on two sides from the neck, whereas in the planar sections it diminishes, although not to zero even at the ends owing to the conservation of mass. The difference of radial velocity between two monolayers is comparatively small throughout the fusion pore–planar section complex. Not only the maximal velocity magnitude, but also the mean velocity (estimated at the end of each monolayer or over the whole monolayer) rises as the pore dilates. As a result the lipid mass flow depends supra-linearly on the pore radius. If mean lipid velocity had been independent of pore radius the lipid mass flow vs. pore radius relationship would have been linear.

Given the small dimensions of the fusion pore–membrane complex and high lipid velocity gradients the viscous and frictional dissipations could be high and need to be evaluated. The frictional dissipation is physically attributed to the friction between the methyl-terminal portions of the acyl chains of the phospholipids [31], and can be further and significantly increased by trans-membrane proteins. The frictional dissipation is proportional by the squared lipid velocity difference at the interface between two monolayers, and the friction coefficient has been measured as a mechanical force needed to pull the leaflets of a bilayer so they slip past one another through a region of high curvature [14,32,33]. Alternatively the bottom monolayer of a membrane was fixed to a glass substrate and the friction coefficient was deduced from the diffusion of tracer lipids in the top monolayer

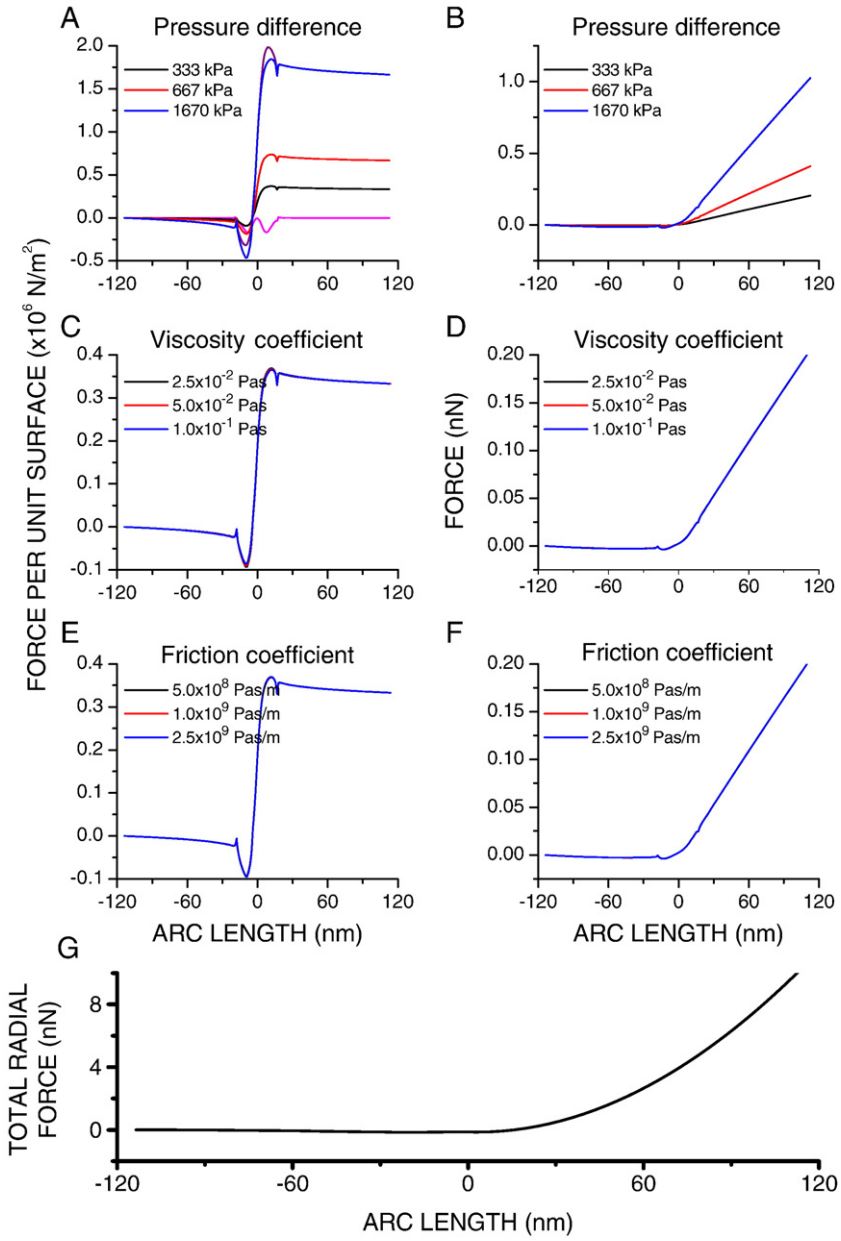

Fig. 10. (A) Radial force per unit area distributions at the external boundary of the outer monolayer. The viscotic (magenta) and pressure (purple) contributions to the radial force per unit surface area, for the simulation with the highest pressure difference at the ends of individual monolayers, are also shown for comparison. Note that the pressure contribution clearly dominates. (B) Corresponding radial force distributions. Whereas the radial force remains zero in the lower ('plasma membrane') planar section irrespective of the pressure difference at the ends of individual monolayers, it increases linearly with distance from the pore center in the upper ('vesicular') section, and the slope increases with the pressure difference. (C–F) Neither the radial force per unit length nor radial force is affected by the changes of the viscosity or friction coefficients. (G) Total radial force at the external boundary of the outer monolayer. The abscissa gives the distance from the end of the plasma membrane. The pressure difference at the ends of individual monolayers was 333 kPa, viscosity coefficient was $5*10^{-2}$ Pa s and the friction coefficient was $5.0*10^8$ Pas/m.

[34]. Its value is typically between 10^8–10^9 Pa s/m^{-1}. The inter-monolayer friction coefficient is not necessarily the same in all tissues, and is expected to be sensitive to the asymmetry of the phospholipids tails, increasing as asymmetry and inter-digitation of the longer tails of two membrane leaflets rise [17]. Finally, the friction between monolayers converts the kinetic energy of sliding at the interface into vibrations of phospholipids (translational or rotational) and into thermal energy, although the detailed mechanisms of this process remain unclear. The potential functional significance of frictional (and viscous dissipation) is to counterbalance the external force (tension or pressure difference).

The frictional dissipation is proportional to the frictional coefficient and squared lipid velocity at the surface where two monolayers slide past each other ([14]; see Appendix). It is thus not surprising that: a) it rises supra-linearly as the pressure difference increases (lipid velocity rises linearly with pressure difference), b) a ten-fold rise of the viscosity coefficient leads to a hundred-fold decrease of the frictional dissipation; the same change leads to the proportional (ten-fold) reduction of the lipid velocity, and c) it rises linearly as the friction coefficient rises, although such a change has no effect on the fluid velocity, pressure, shear and normal stresses as well as viscous dissipation. Under conditions expected to occur physiologically the frictional dissipation is much smaller than the viscous dissipation, but it rises (approximately linearly) but significantly as the pore radius increases. Finally, note that in the previous theoretical and largely analytical study, it was assumed that in the planar section the membranes do not slide past each other, and that thus there the frictional dissipation is zero [14]. This study confirms the validity of

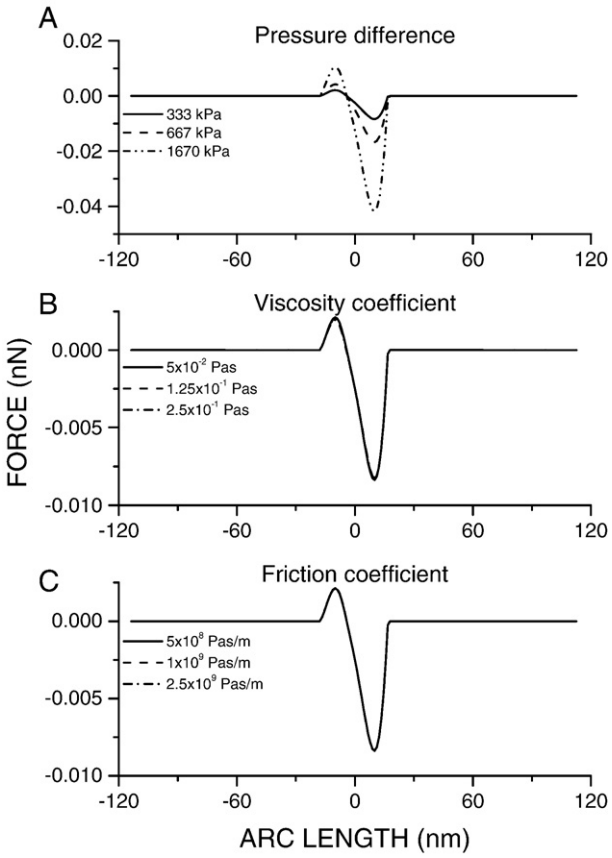

Fig. 11. (A) Axial force, which is much smaller than the radial force, is confined to the toroidal section. Note that in the lower part of the toroidal section it is very small but positive, whereas in the upper part it is greater but negative. The axial force depends on the pressure difference at the ends of individual monolayers. (B, C) Altering the viscosity or friction coefficients has no effect on the axial force.

this assumption, and demonstrates moreover that the frictional dissipation is not only confined to the toroidal section, but is within the toroid highly localized at the pore neck.

4.2. Normal and shear stresses

The spatial distribution of the normal stress tells us where the membrane may compress or extend (i.e. where its volume will change), and the compression–extensions in radial and axial directions are both of interest. The radial normal stress is localized largely in the toroidal section, and the values in two monolayers are similar. The axial normal stress is however confined exclusively at the neck of the toroidal section, and it is typically greater in the outer monolayer. The localization of the normal stress is not surprising given the geometry of the fusion pore and definition of the normal stress (axial and radial; see Methods). The shear stress suggests where the membrane will deform without changing the volume. The shear stress changes rapidly in the toroidal section, and is zero at the pore neck, which is positioned parallel to the axis of symmetry, and where an element of the membrane volume does not deform. Moving from the pore center the shear stress rapidly rises, forming two peaks, which are placed symmetrically from the central point of no dissipation and diminishes to zero value in the planar membrane. Their locus of the shear peaks is determined from the interplay of shear deformation caused by the radial and angular positioning of a membrane volume element. The shear and normal (axial and radial) stresses are all controlled by the pressure difference, whereas the changes of the viscosity and frictional coefficients have only a minimal effect.

4.3. Viscous dissipation

The viscous dissipation per unit volume gives the rate at which mechanical energy is converted into heat. Viscous dissipation effects are significant when fluid velocity is high and flows are highly viscous. In macrosize systems this issue does not become serious frequently, but in nanosize systems such as the fusion pore–membrane complex the fluid velocity and its gradients become elevated easily. It is thus not surprising that in the toroidal section, where the lipid velocity and its gradients (which determine the viscous dissipation; see Appendix), are also the greatest the viscous dissipation is pronounced. The distribution of the viscous dissipation is wider, because the volume for which the viscous dissipation is calculated increases as the distance from the fusion pore center rises. How large the viscous dissipation is, is controlled by the pressure difference and by the viscosity coefficient, which reflects molecular interactions within individual monolayer [31]. The viscosity coefficient depends on whether the membrane is a cell membrane or a lipid bilayer. One critical element appears to be the combined lengths of the two lipid tails, rather than their asymmetry [15]. The coefficient may also depend on a variety of physiological conditions. Addition of cholesterol and/or lower temperature, which increases the ordering of the lipids and slows the lateral diffusion [35,36], also renders the viscosity coefficient higher. We thus evaluated the dynamics of the lipid flow over a range of viscosity coefficients. Raising the viscosity coefficient leads to a proportional reduction of the lipid velocity and of the viscous dissipation. Note however, that the addition of cholesterol changes the membrane curvature [37], and that is not included in our simulations. Such an effect would change the lipid velocity and other variables determined by the lipid velocity. Finally note that both viscous and frictional dissipations, which counterbalance the external force (tension or pressure difference), would also affect the rate of membrane deformation and its recovery promoted by the elastic restoring forces in the membrane.

4.4. Pressure and force acting on the fusion pore–membrane complex

Difference in tension between vesicular and plasma membranes is simulated as a difference in pressure at two ends of each monolayer, using the relationship between the tension and pressure as given previously ([40]; see Appendix). The pressure difference is the driving force causing the lipid flow and has a major effect on all variables. Its spatial profile is simple. The pressure, which is similar in two monolayers, changes only modestly in the planar sections, whereas in the toroidal section the change is rapid. More importantly the pressure is near zero in the lower planar section ('plasma membrane'), and high in the upper planar section ('vesicular membrane'), but how high it is depends on the pressure difference at the ends of the monolayers.

The radial force determines how much and how rapidly the fusion pore will dilate. The radial force per unit area is close to zero in the lower planar section ('plasma membrane'), rises rapidly in the toroidal section to a new value, which remains essentially constant in the upper planar section ('vesicular membrane'), and is largely determined by pressure difference at the ends of the monolayers. As a consequence the radial force, which is also essentially zero in the plasma membrane, rises linearly with distance from the fusion pore center in the vesicular membrane. These simulations thus demonstrate that following the fusion of the vesicular and plasma membranes the vesicular membrane will dilate whereas the plasma membrane will remain unaffected. The axial force, which is much smaller than radial force, is near zero value in plasma and vesicular membrane sections, but in the toroidal section it is negative in the lower and positive in the upper section. The fusion pore should thus dilate only radially whilst the axial dilatation should be only marginal. Finally note that assuming that the vesicular membrane tension is

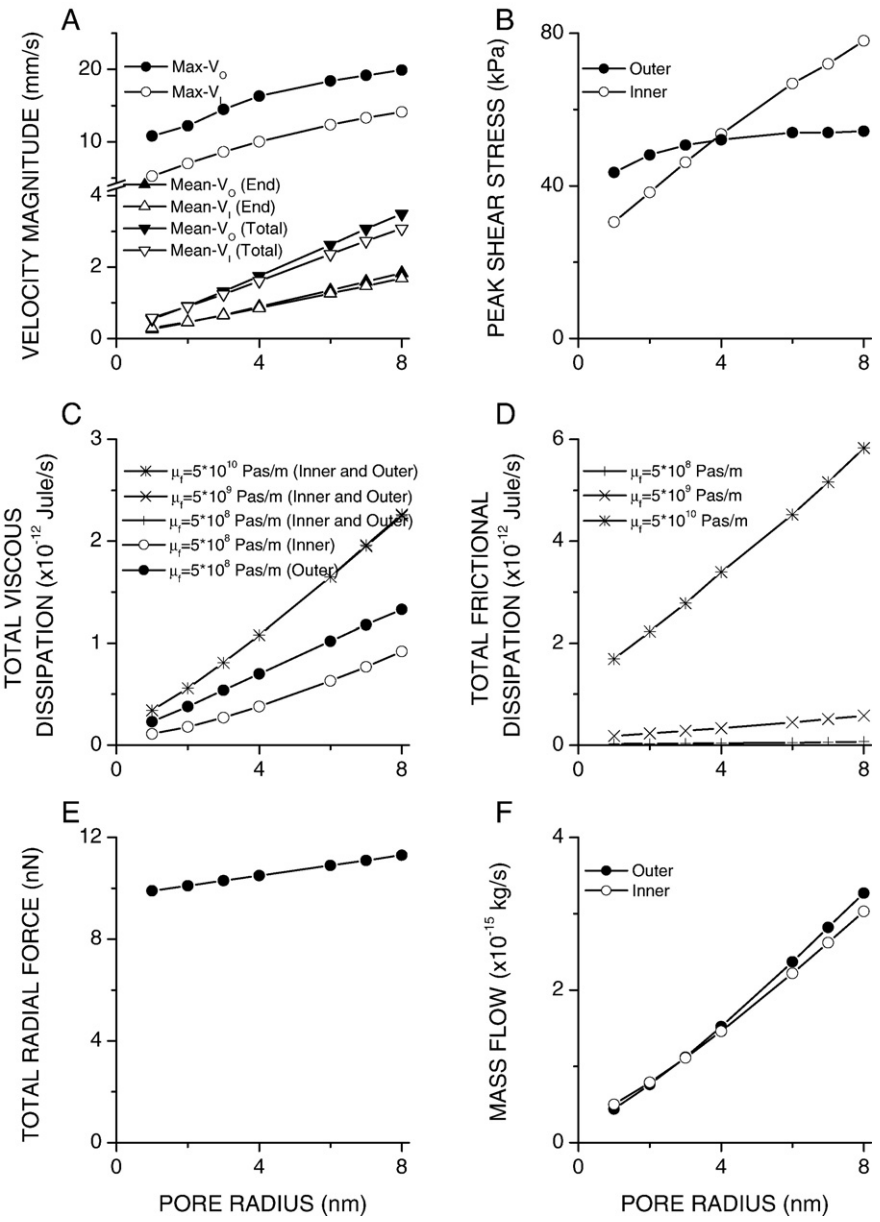

Fig. 12. Fusion pore dilatation alters many, but not all variables determining the lipid flow. (A) The maximal toroidal velocity magnitude, which is greater in the outer monolayer, rises approximately linearly as the pore dilates. Mean velocity magnitude at the end of individual monolayers and mean total velocity magnitude (averaged over the whole volume of each monolayer) also rise linearly with pore dilatation. (B) The peak value of the shear stress in the toroid rises modestly in the outer monolayer but more so in the inner monolayer. (C) Total viscous dissipation, which is greater in the outer monolayer, rises approximately linearly with dilatation and is not affected even by great increases of the frictional coefficient μ_f. (D) Total frictional dissipation, which increases as the pore dilates, is only a small fraction of the total viscous dissipation at 'physiological' level of the frictional coefficient ($\mu_f = 5*10^9$ Pa s/m), but increases markedly as μ_f rises. (E) Total radial force rises but only modestly with dilatation. (F) Lipid mass flow increases supra-linearly with dilatation owing to the greater velocity in wider pores (see text). The lipid mass flow is only marginally greater in the outer monolayer and only when the pore is wide.

independent of vesicular radius the dilatation force will be larger for pores of wider radius, although not greatly. They would thus open faster and release their content faster and this may also selectively increase their probability of release. This could serve as a compensatory mechanism. If all vesicles irrespective of their size had the same fusion pore radius the larger vesicles would release their content much more slowly owing to the less favorable ratio of the cross-sectional area of the fusion pore and the total surface area of vesicle [39].

4.5. Future directions

This study is based on the assumption that the lipid is homogeneous and isotropic. The monolayer is however, not a simple bulk liquid because within the monolayer the lipids are straightened, oriented, and ordered. Nevertheless the radial force (and thus pore dilation) is unlikely to be affected by the anisotropy, which is significant only in the upper membrane section ('vesicular membrane'), and which is planar. However, such an anisotropy may have other effects and a detailed study is needed to assess what they are. Finally this study evaluates only the stationary lipid flow and the stresses and forces generated by the tension difference between the vesicular and plasma membranes. It would be highly desirable to expand its scope with time-dependent simulations, and also by determining the membrane deformation [38], which results from the pressure difference that produces the lipid flow and generates the stresses and forces acting on the fusion pore–membrane complex.

5. Conclusion

We simulated the stationary convective flux of lipid through a fusion pore connecting two planar membranes under different tensions using methods of computational fluid dynamics to estimate the lipid velocity, shear and normal stresses, viscous and frictional dissipations in the membrane and forces acting on the fusion pore during secretion. The pressure difference at the ends of individual monolayers drives the lipid flow, determines lipid velocity and velocity dependent variables (shear as well as normal axial and radial stresses), and contributes directly to the force on the membranes critically influencing where and to what extent the membrane will deform, extend or dilate. The radial force, which indicates whether and if so where the membrane pore will dilate, is very low in the plasma membrane, but can be large in the vesicular membrane. The radial force increases linearly with the distance from the pore center and is thus greater for larger vesicles, but increases only marginally with pore dilatation.

Appendix

System equations

We consider the system in 2D r–z plane of the cylindrical coordinate system ignoring the velocity and its gradient in θ direction. The simplified Navier–Stokes equation in terms of components of the stress tensor $\boldsymbol{\tau}$ thus reads as follows:

$$r-\text{component}: \rho\left(\frac{\partial u}{\partial t}+u\frac{\partial u}{\partial r}+v\frac{\partial u}{\partial z}\right)=-\frac{\partial p}{\partial r}-\left[\frac{1}{r}\frac{\partial}{\partial r}(r\tau_{rr})+\frac{\partial \tau_{rz}}{\partial z}\right] \tag{3}$$

$$z-\text{component}: \rho\left(\frac{\partial v}{\partial t}+u\frac{\partial v}{\partial r}+v\frac{\partial v}{\partial z}\right)=-\frac{\partial p}{\partial z}-\left[\frac{1}{r}\frac{\partial}{\partial r}(r\tau_{rz})+\frac{\partial \tau_{zz}}{\partial z}\right] \tag{4}$$

where u and v are the r- and z-components of the fluid velocity, respectively. τ_{ij} are the ij-th components of the viscous stress tensor $\boldsymbol{\tau}$, which for Newtonian fluids in 2D r–z plane (of the cylindrical coordinate system) are defined as:

$$\tau_{rr}=-\mu\left[2\frac{\partial u}{\partial r}-\frac{2}{3}(\nabla.\mathbf{u})\right] \tag{5}$$

$$\tau_{zz}=-\mu\left[2\frac{\partial v}{\partial z}-\frac{2}{3}(\nabla.\mathbf{u})\right] \tag{6}$$

$$\tau_{rz}=-\mu\left[\frac{\partial v}{\partial r}+\frac{\partial u}{\partial z}\right] \tag{7}$$

where

$$\nabla.\mathbf{u}=\frac{1}{r}\frac{\partial}{\partial r}(ru)+\frac{\partial v}{\partial z}. \tag{8}$$

With substitution of the components of the stress tensor, Eqs. 5–8, into the Eqs. 3–4 and constant ρ and μ, we will reach to Eqs. 9–10 describing the Navier–Stokes equation in terms of velocity gradients, which are computationally friendly.

$$r-\text{component}: \rho\left(\frac{\partial u}{\partial t}+u\frac{\partial u}{\partial r}+v\frac{\partial u}{\partial z}\right)=-\frac{\partial p}{\partial r}+\mu\left[\frac{\partial}{\partial r}\left(\frac{1}{r}\frac{\partial}{\partial r}(ru)\right)+\frac{\partial^2 u}{\partial z^2}\right] \tag{9}$$

$$z-\text{component}: \rho\left(\frac{\partial v}{\partial t}+u\frac{\partial v}{\partial r}+v\frac{\partial v}{\partial z}\right)=-\frac{\partial p}{\partial z}+\mu\left[\frac{1}{r}\frac{\partial}{\partial r}\left(r\frac{\partial v}{\partial r}\right)+\frac{\partial^2 u}{\partial z^2}\right]. \tag{10}$$

Force on fusion pore membrane

The z-axis is considered as the axis of symmetry, and therefore the transient Navier–Stokes equation of motion in the absence of external forces can be rearranged as:

$$r\rho\frac{\partial \mathbf{u}}{\partial t}+\nabla.\boldsymbol{\tau}=\mathbf{F} \tag{11}$$

where r is the distance from z-axis, ρ is the fluid density, $\mathbf{u}=(u_r,u_z)=(u,v)$ is the velocity vector, $\boldsymbol{\tau}$, and $\mathbf{F}$ are the viscous stress tensor and the total force acting on a control volume, respectively. Their compact matrix notations are as follows:

$$\boldsymbol{\tau}=-r\mu\begin{bmatrix}2\frac{\partial u}{\partial r} & \frac{\partial u}{\partial z}+\frac{\partial v}{\partial r}\\ \frac{\partial u}{\partial z}+\frac{\partial v}{\partial r} & 2\frac{\partial v}{\partial z}\end{bmatrix}\text{ and }\quad \mathbf{F}=-\begin{bmatrix}r\left(\rho\left(u\frac{\partial u}{\partial r}+v\frac{\partial u}{\partial z}\right)+\frac{\partial p}{\partial r}\right)+\frac{2\mu}{r}u\\ r\left(\rho\left(u\frac{\partial v}{\partial r}+v\frac{\partial v}{\partial z}\right)+\frac{\partial p}{\partial z}\right)\end{bmatrix}. \tag{12}$$

The force is calculated from the total stress tensor ($\mathbf{T}$), which comprises the pressure and viscous stress tensor as the following:

$$\mathbf{T}=-p\mathbf{I}+\boldsymbol{\tau} \tag{13}$$

where $\mathbf{I}$ is the unity tensor. The total force acting on surfaces of the monolayers is then given by the following equation:

$$F_i=\oint T_{ij}dS_j \tag{14}$$

where the component T_{ij} of the total stress tensor is the i-th component of the force applied to a unit area perpendicular to the x_j axis.

Viscous and frictional dissipations

The viscous dissipation per unit volume is written as $\mu\phi_v=\boldsymbol{\tau}:\nabla\mathbf{u}$ where ϕ_v for a Newtonian fluid is given below in the cylindrical coordinate system.

$$\phi_v=2\left[\left(\frac{\partial u}{\partial r}\right)^2+\left(\frac{u}{r}\right)^2+\left(\frac{\partial v}{\partial z}\right)^2\right]+\left[\frac{\partial u}{\partial z}+\frac{\partial v}{\partial r}\right]^2-\frac{2}{3}(\nabla.\mathbf{u})^2. \tag{15}$$

Note that Eq. (15) is derived assuming that the velocity and its gradient in the θ-direction are zero.

Energy dissipation due to friction, $\dot{e}_f$, at the interface between two sliding lipid monolayers is given as described previously [14]:

$$\dot{e}_f=\mu_f\int(\Delta\mathbf{u})^2 dS \tag{16}$$

where $\Delta\mathbf{u}$ is the velocity difference along the interfacial surface, S, between two monolayers that slide past each other.

All simulations were done using a commercial finite element method (FEM) program Comsol 3.4 (Comsol, Burlington, MA, USA), whereas the post-processing was performed using Matlab (MathWorks, Natick, MA, USA) a software package for scientific and engineering computing. All graphics were made with Origin (Microcal Software, Northampton, MA, USA).

Tension difference is simulated as pressure difference

As already stated each monolayer is considered as an incompressible fluid and is simulated using Navier–Stokes equations defined in terms of fluid velocity and pressure. Notice however, that the external force – the pressure difference at the ends of each monolayer – is calculated from the experimentally measured tension difference of

vesicular and plasma membranes, and the relationship is given by Laplace's Law as follows [40]:

$$\gamma = \int_{h1}^{h2} [P_N(n) - P_T(n)]dn \quad (17)$$

where γ is the surface tension of the lipid bilayer with the thickness $h = h_2 - h_1$ and n is normal to the surface. P_N and P_T are respectively the normal and tangential components of pressure to the surface. If we consider the surface at the mechanical equilibrium and assuming $P_N = P_0$ and equal to the constant atmospheric pressure, the above equation becomes:

$$\gamma = \int_{h1}^{h2} [P_0 - P_T(n)]dn. \quad (18)$$

References

[1] W. Almers, Exocytosis, Annu. Rev. Physiol. 52 (1990) 607–624.
[2] M.I. Glavinović, Monte Carlo simulation of vesicular release, spatiotemporal distribution of glutamate in synaptic cleft and generation of postsynaptic currents, Pflugers Arch. - Eur. J. Physiol. 437 (1999) 462–470.
[3] D. Sulzer, E.N. Pothos, Regulation of quantal size by presynaptic mechanisms, Rev. Neurosci. 11 (2000) 159–212.
[4] L.J. Breckenridge, W. Almers, Currents through the fusion pore that forms during exocytosis of a secretory vesicle, Nature 328 (1987) 814–817.
[5] J. Zimmerberg, M. Curran, F.S. Cohen, A lipid/protein complex hypothesis for exocytotic fusion pore formation, Ann. N.Y. Acad. Sci. 635 (1991) 307–317.
[6] C. Nanavati, V.S. Markin, A.F. Oberhauser, J.M. Fernandez, The exocytotic fusion pore modeled as a lipidic pore, Biophys. J. 63 (1992) 1118–1132.
[7] M. Lindau, W. Almers, Structure and function of fusion pores in exocytosis and ectoplasmic membrane fusion, Curr. Opin. Cell Biol. 7 (1995) 509–517.
[8] L.V. Chernomordik, M.M. Kozlov, J. Zimmerberg, Lipids in biological membrane fusion, J. Membr. Biol. 146 (1995) 1–14.
[9] L.D. Hernandez, L.R. Hoffman, T.G. Wolfsberg, J.M. White, Virus–cell and cell–cell fusion, Annu. Rev. Cell Dev. Biol. 12 (1996) 627–661.
[10] B.P. Jena, S.J. Cho, A. Jeremic, M.H. Stromer, R. Abu-Hamdah, Structure and composition of the fusion pore, Biophys. J. 84 (2003) 1337–1343.
[11] X. Han, M.B. Jackson, Structural transitions in the synaptic SNARE complex during Ca2+-triggered exocytosis, J. Cell Biol. 172 (2006) 281–293.
[12] J.R. Monck, G. Alvarez de Toledo, J.M. Fernandez, Tension in secretory granule membranes causes extensive membrane transfer through the exocytotic fusion pore, Proc. Natl. Acad. Sci. U.S.A.. 87 (1990) 7804–7808.
[13] C. Solsona, B. Innocenti, J.M. Fernandez, Regulation of exocytotic fusion by cell inflation, Biophys. J. 74 (1998) 1061–1073.
[14] Y.A. Chizmadzhev, D.A. Kumenko, P.I. Kuzmin, L.V. Chernomordik, J. Zimmerberg, F. Cohen, Lipid flow through fusion pores connecting membranes of different tensions, Biophys. J. 76 (1999) 2951–2965.
[15] W.K. den Otter, S.A. Shkulipa, Intermonolayer friction and surface shear viscosity of lipid bilayer membranes, Biophys. J. 93 (2007) 423–433.
[16] U. Seifert, S.A. Langer, Viscous modes of fluid bilayer membranes, Europhys Lett. 23 (1993) 71–76.
[17] S.A. Shkulipa, W.K. den Otter, W.J. Briels, Surface viscosity, diffusion, and intermono-layer friction: simulating sheared amphiphilic bilayers, Biophys. J. 89 (2005) 823–829.
[18] P.G. Saffman, Brownian motion in thin sheets of viscous fluid, J. Fluid Mech. 73 (1976) 593–602.
[19] R.E. Waugh, Surface viscosity measurements from large bilayer vesicle tether formation. II. Experiments, Biophys. J. 38 (1982) 29–37.
[20] M.J. Saxton, K. Jacobson, Single particle tracking: applications to membrane dynamics, Annu. Rev. Biophys. Biomol. Struct. 26 (1997) 373–399.
[21] K. Velikov, C. Dietrich, A. Hadjiisky, K. Danov, B. Pouligny, Motion of a massive microsphere bound to a spherical vesicle, Europhys. Lett. 40 (1997) 405–410.
[22] R. Dimova, C. Dietrich, A. Hadjiisky, K. Danov, B. Pouligny, Falling ball viscosimetry of giant vesicle membranes: finite-size effects, Eur. Phys. J. B. 12 (1999) 589–598.
[23] R. Dimova, B. Pouligny, C. Dietrich, Pretransitional effects in dimyristoyl-phosphatidylcholine vesicle membranes: optical dynamometry study, Biophys. J. 79 (2000) 340–356.
[24] P. Cicuta, S.L. Keller, S.L. Veatch, Diffusion of liquid domains in lipid bilayer membranes, J. Phys. Chem. B. 111 (2007) 3328–3331.
[25] F. Julicher, A. Ajdari, J. Prost, Modeling molecular motors, Rev. Mod. Phys. 69 (1997) 1269–1281.
[26] Y. Tang, G. Cao, X. Chen, J. Yoo, A. Yethiraj, Q. Cui, A finite element framework for studying the mechanical response of macromolecules: application to the gating of the mechanosensitive channel MscL, Biophys. J. 91 (2006) 1248–1263.
[27] R. Qiao, N.R. Aluru, Ion concentrations and velocity profiles in nanochannel osmotic flows, J. Chem. Phys. 118 (2003) 4692–4701.
[28] G. De Luca, M.I. Glavinović, Glutamate, water and ion transport through a charged nanosize pore, Biochim. Biophys. Acta - Biomemb. 1768 (2007) 264–279.
[29] V.A. Frolov, V.A. Lizunov, A.Y. Dunina-Barkovskaya, A.V. Samsonov, J. Zimmerberg, Shape bistability of a membrane neck: a toggle switch to control vesicle content release, Proc. Natl. Acad. Sci. U.S.A. 100 (2003) 8698–8703.
[30] R.B. Bird, W.E. Stewart, E.N. Lightfoot, Transport Phenomena, Wiley, 1960.
[31] E.A. Evans, R.M. Hochmuth, Mechanochemical properties of membranes, Curr. Top. Membr. Transp. 10 (1978) 1–62.
[32] E.A. Evans, A. Young, Hidden dynamics in rapid changes in bilayer shape, Chem. Phys. Lipids 73 (1994) 39–56.
[33] R.M. Raphael, R.E. Waugh, Accelerated interleaflet transport of phosphatidylcholine molecules in membranes under deformation, Biophys. J. 71 (1996) 1374–1388.
[34] R. Merkel, E. Sackmann, A. Evans, Molecular friction epitatic coupling between monolayers in supported bilayers, J. Phys. (France). 50 (1989) 1535–1555.
[35] W.L.C. Vaz, R.M. Clegg, D. Hallmann, Translational diffusion of lipids in liquid crystalline phase phosphatidylcholine multibilayers. A comparison of experiment with theory, Biochemistry 24 (1985) 781–786.
[36] A. Filippov, G. Oradd, G. Lindblom, The effect of cholesterol on the lateral diffusion of phospholipids in oriented bilayers, Biophys. J. 84 (2003) 3079–3086.
[37] M.A. Churchward, T. Rogasevskaia, D.M. Brandman, H.K.P. Nava, J.K. Atkinson, J.R. Coorssen, Specific lipids supply critical negative spontaneous curvature — an essential component of native Ca21-triggered membrane fusion, Biophys. J. 94 (2008) 3976–3986.
[38] W. Helfrich, Elastic properties of lipid bilayers — theory possible experiments, Z. Naturforsch. [C]. 28 (1973) 693–703.
[39] H.R. Rabie, J. Rong, M.I. Glavinović, Monte Carlo simulation of release of vesicular content in neuroendocrine cells, Biol. Cybern. 94 (2006) 483–499.
[40] S.H. White, Small phospholipid vesicles: internal pressure, surface tension, and surface free energy, Proc. Natl. Acad. Sci. U.S.A. 77 (1980) 4048–4050.